Renewable Energy 239 (2025) 122185

Contents lists available at ScienceDirect

Renewable Energy

journal homepage: www.elsevier.com/locate/renene

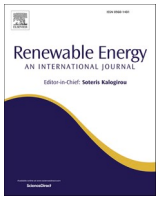

Comprehensive performance analysis of a novel closed-loop hydronic cooling of photovoltaic panel with a controlled intermittent flow strategy

Hazim Dirawi [a], Qiliang Wang [a,*], Mingke Hu [b], Yuehong Su [a,**], Saffa Riffat [a]

[a] Architecture and Built Environment Department, University of Nottingham, University Park, Nottingham, NG7 2RD, UK
[b] School of Electrical Engineering, Southwest Jiaotong University, Chengdu, 610031, China

ARTICLE INFO

Keywords:
Photovoltaic (PV)
Closed-loop hydronic cooling
Controlled intermittent flow (CIF)
PV temperature
Net power production
Lifetime

ABSTRACT

Photovoltaic (PV) technology has seen rapid development in hot and arid regions due to intense solar radiation. However, extreme weather conditions pose challenges for PV applications in terms of efficiency and lifespan. A new closed-loop hydronic cooling system for PV panels, designed for 24-h continuous operation, was developed to address these challenges. However, a circulation pump can consume a considerable amount of electricity due to 24-h continuous operation, resulting in substantial wastage. This study proposes a controlled intermittent flow (CIF) strategy for the pump to optimize operation hours and minimize energy consumption under favourable PV temperature conditions. A dynamic 3D simulation model was developed and validated to numerically analyse the performance metrics of the proposed PV cooling method with CIF. The yearly performance of PV panel cooling systems with continuous flow (CF) and CIF, as well as common PV panels, was comprehensively evaluated and compared. The results showed that the CIF strategy effectively reduces the pump's operating hours and energy consumption while minimally impacting the system's net electricity output. The CIF strategy is found to yield a significant enhancement in seasonal net power output, with a 0.57 % increase during winter and a 0.83 % increase in summer compared to the CF system. Moreover, employing the CIF strategy with a setpoint of 35 °C results in a consistent 0.96 % rise in annual net power output across all months compared to the CF system, except for the lifespan, the CF is better. For Basra's local climatic condition in Iraq, the CF and CIF closed-loop photovoltaic cooling systems show significant lifetime improvements of up to 34.3 % and 41 % over common PV panels, while for Hong Kong's local climatic condition, the CIF system outperforms by 4.9 % and 22.2 % compared to CF system and common PV panel, respectively. The proposed closed-loop hydronic cooling method for PV panels with CIF exhibits the best performance among the three types of PV systems, making it particularly suitable for regions with hot and arid climates.

1. Introduction

Renewable energy sources are progressively becoming more popular nowadays due to concerns about the sustainability and pollution of common energy sources. The solar energy stands as one of the most freely available and reliable sources nowadays. One type of renewable and environmentally friendly energy is the usage of photovoltaic (PV) panels, which convert sunlight into electrical energy. The efficiency of PV systems is affected by a variety of factors such as solar cell temperature, solar irradiation, ambient temperature, and weather conditions. In hot and dry environments, the solar cell surface temperature reaches about 125 °C [1], which not only reduces the efficiency of PV systems [2] but also subjects the PV panels to higher thermal stress, significantly shortening their lifespan [3–6]. As a result, a cooling system is required to maintain and lower the temperature of the PV system to enhance its lifespan and efficiency.

PV cooling technologies have been extensively researched by numerous studies to cool it down and enhance its performance. Several methods for cooling (active or passive) are described in the researched literature, including water cooling [7], air cooling [8], phase change material-based [9], heat pipe-based [10], and thermoelectric cooling [11]. The cooling techniques can be classified by the type of coolant fluid, the efficiency of heat transfer, temperature characteristics, and the intended application of the system (non-concentrated or concentrated)

* Corresponding author.
** Corresponding author.
E-mail addresses: qiliang.wang1@nottingham.ac.uk (Q. Wang), yuehong.su@nottingham.ac.uk (Y. Su).

https://doi.org/10.1016/j.renene.2024.122185
Received 1 September 2024; Received in revised form 10 December 2024; Accepted 15 December 2024
Available online 15 December 2024

[12]. Photovoltaic (PV) cooling systems utilizing water as a cooling medium offer several advantages. Firstly, water is an environmentally benign working fluid that does not contribute to contamination, and it possesses a high cooling capacity. Moreover, water is readily available and is commercially cost-effective. Kluth [13] investigated water as a cooling fluid to improve PV efficiency. In this study, two small-scale PV panel models were developed: one model operated without cooling, while the other was subjected to water cooling via a blower-assisted spray. It was discovered that PV panels using water cooling produce more energy than those without any cooling. Nevertheless, cooling via spraying water using a fan isn't efficient because the water isn't sprayed through the entire PV panels and hence some places of the panel are uncooled; additionally, this approach results in significant water loss.

In such contexts, utilizing a control flow approach in PV cooling systems can enhance pump operation, leading to improved energy efficiency and reduced operational costs. Hadipour et al. [14] investigated the performance of water pulsed-spray and steady-spray cooling methods for PV modules. The results indicated that the pulsed-spray cooling technique utilized just about 10 % of the water utilized by the steady-spray technique. As a result of the significant reduction in water consumption, the PV system with pulsed-spray cooling had a 76 % lower levelized cost of energy than the PV panel with steady-flow cooling. A detailed study in Ref. [15] employed a dynamic optimisation technique to control and enhance the water flow rate utilized in the front water cooling of PV panels, aiming to minimize water usage while simultaneously maximizing electrical output. Their calculations revealed that with the appropriate flow rate, the average and peak temperatures of the water-cooling PV panel could be reduced by 54 % and 61 %, respectively, when compared with a PV panel without any water-cooling mechanism. While pulsed spray cooling significantly reduces water wastage compared to continuous spray cooling, it remains impractical in hot, arid regions due to the need for continuous replenishment caused by high evaporation rates [13–15]. Moreover, this front surface cooling can obstruct incoming solar radiation, thereby decreasing the photovoltaic efficiency.

Aiming to achieve a water-saving and efficient PV cooling system in hot arid regions, a novel closed-loop hydronic cooling of PV panels with a controlled intermittent flow (CIF) strategy was proposed in this study to regulate the PV overheating issue with a minimising amount of water and pump power consumption. Utilizing designated temperature thresholds, enhancing panel efficacy, and adapting to varying environmental conditions are key strategies employed in this approach, leading to decreased maintenance requirements and the promotion of sustainable resource utilization. Ultimately, these measures serve to enhance system performance and cost-effectiveness.

This study proposes an automated system for controlling water flow rates in hot arid regions like Iraq using a closed-loop PV cooling system. Controlled intermittent flow (CIF) is an energy-saving solution, allowing pump switching. 3D simulations are used to investigate CIF characteristics and the effects of cooling CIF and continuous flow (CF) on total and net electrical power output. By using this model, it is possible to determine the optimal timing to commence cooling of the PV panels. The validation of the model has been verified with experimental data measured on the June 2, 2024 at the University of Nottingham, UK. This study has been selected to examine the effects of CIF on the performance of PV modules in this investigation. The primary emphasis is placed on comparing and evaluating the efficiency of the PV module and net output power with and without a cooling system. The second objective of this study is to assess the impact of different weather conditions on CIF output parameters, such as pump working hours and net power, across various seasons and climate conditions. The remaining parts of this paper are divided into the following sections. The next section provides a comprehensive system overview, encompassing the PV design and the experimental configuration employed for the validation of the numerical simulation method. The following section elaborates on the PV model's methodology, which includes the governing equations and the numerical procedures implemented. Subsequently, the principal findings and discussions pertaining to this research are presented. The final section articulates the conclusions drawn and their broader implications. The study discovered that the CIF technique decreases pump working hours and energy consumption while increasing seasonal net power output by 0.57 % in winter and 0.83 % in summer, compared to the CF system. The closed-loop hydronic cooling for PV panels with CIF is demonstrated to be the most effective and optimal for hot and dry climates.

2. System description

2.1. PV cooling system

The common photovoltaic (PV) panels comprise a transparent glass layer, solar cells, and two layers of EVA with a protective backing layer. Compared to a common PV module, the proposed closed-loop hydronic cooling of a PV system comprises a PV panel of several layers, a storage tank, water channels and a pump for circulation as illustrated in Fig. 1. The PV panel comprises transparent glass, monocrystalline silicon cells, an aluminium absorber plate as well as water tubes mounted beneath the aluminium layer. The effective area of the PV panel for collecting solar radiation is $1.475 \times 0.67\ m^2$ and the cell area is $0.848\ m^2$. The PV module consists of 36 individuals of cells and a packing factor of 0.858 with 15 % conversion efficiency. In this study, a 150 L water storage tank is used, creating a full closed-loop with a PV module and the pump connected via copper tubes. Due to the high environmental temperature and strong solar irradiation in hot regions, the proposed solar PV panel design eliminates any insulating layer from the tubes and water tank on purpose. This allows heating energy to be released, avoiding the water from attaining a high temperature and thereby affecting PV efficiency. Furthermore, the lack of insulation increases heat loss during nocturnal discharge, providing adequate cooling of the working fluid. This is beneficial for efficiently cooling the solar cells throughout the daytime.

On this structure, the bottom side of the PV module is fitted by two manifolds with eight pipes, which allow water to flow inside to heat and cool the panel during the night and daytime, accordingly. The tube and manifold have diameters of 15 mm and 22 mm, respectively. The water tube configuration offers that each solar cell row has a minimum of one water tube underneath it, which allows for efficient cooling. Detailed data about the dimensions, thermophysical specifications and spectral properties of the different layers that comprise the PV module can be obtained from Table 1.

2.2. Experimental setting and procedure

This section provides details on the experimental configuration for the study. The experimental arrangement was carefully designed to minimize water loss. The study was carried out in June 2024, during the summer period in Nottingham, UK, at the University of Nottingham (52.95° N and 1.16° E). The system operated for several days with a controlled water flow rate of 1.6 L/min for all measurement cases. The measurement period extended all daytime on June 2nd, 2024, focusing exclusively on sunny days without heavy clouds. Temperature data were recorded with a sequential resolution of 10 s. To assess and analyse the experimental data, average values were determined for 3-h intervals with a time step of 1 min.

In Fig. 2, the system is primarily composed of a PV module, a flowmeter, a 50 L tank, a pump for circulation water, a maximum power point tracking (MPPT) controller, voltage and current sensors, an AC power source, a 12-V storage battery, a pyranometer, platinum resistance, various thermocouples, a valve, thermometer shelter and switches. Moreover, a DataTaker recorded and stored values with a 5-s time resolution step from 13:15 to 16:15. The PV collector was positioned at an inclined angle of 45° towards the country's southern section to receive the maximum solar irradiation as shown in Fig. 2, and the flow

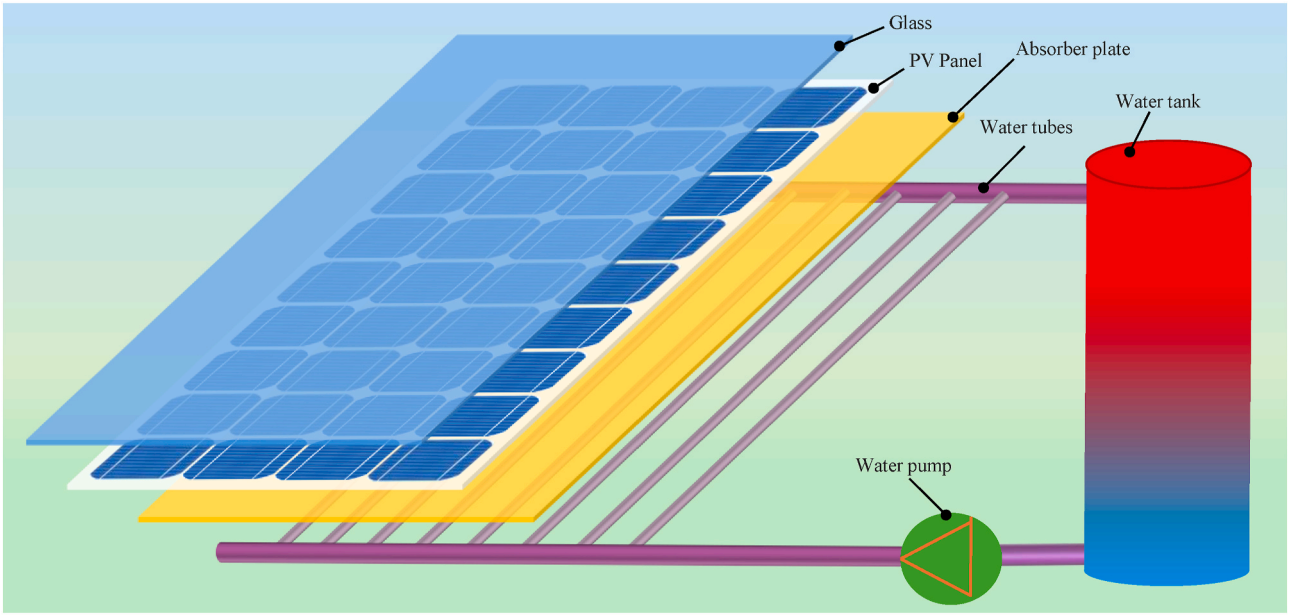

Fig. 1. The schematic structure of the closed-loop hydronic cooling system for the PV panel.

Table 1
Design specifications for each layer of PV module.

Properties	Glass (Top cover)	PV cells (Silicon)	EVA	Aluminium plate	Copper tubes
Density (kg/m^3)	3000	600	1200	917	8933
Thermal conductivity (W/m•K)	1.05	149	0.15	238	401
Heat capacity J/(kg•K)	750	700	1250	917	385
Thickness (mm)	3	3.5	0.4	0.4	0.74
Transmissivity	0.9	–	–	–	–
Absorptivity	0.038	0.925	0.925	–	–
Emissivity	0.88	0.95	–	–	–

rate has been adjusted to 0.027 kg/s. A platinum resistance thermometer was situated inside the shelter to monitor the temperature of ambient. In order to track the outlet-inlet water temperature, two additional thermocouples were mounted at the manifold collector's outlet and inlet. Ten thermocouples were placed on the rear of the PV module to measure panel and copper pipe temperatures, while two other thermocouples were installed in the circulating tank to monitor water temperature. The data logger recorded all measured data at a 10-s interval.

3. Simulation method for the closed-loop PV cooling system

3.1. Governing equations

The basic mathematical model equations for the closed-loop hydronic cooling of the PV panel have been developed to examine its performance within dynamic conditions. The development considers the energy inflow and outflow rates across various layers of the PV module. The temperature of module layers and water storage tanks is calculated using a COMSOL Multiphysics simulation model. Heat transfer equations are generated for each layer using the basic energy equation, allowing for detailed analysis. The momentum, mass balance, and thermal equations are numerically solved utilizing the finite element approach established in the COMSOL. The governing equations for fluid flow in 3D form can be expressed in Eqs. (1)–(3):

The conservation of energy for the fluid flow can be described below [16]:

$$\rho C_p \frac{\partial T}{\partial t} + \rho C_p u \cdot \nabla T = \nabla \cdot (k \nabla T) + .Q \tag{1}$$

where C_p and ρ are the specific heat capacity of fluid (kJ·kg^{-1}·K^{-1}) and density (kg·m^{-3}), accordingly; t describes the time (s) while T denotes the temperature of fluid (K); k and u represent the fluid conductivity (W·m^{-1}·K^{-1}) and velocity (m·s^{-1}), respectively. $\dot{Q}$ quantifies the energy generation rate occurring within system (W·m^{-3}).

The conservation of momentum, taking into account the influence of gravity, could have been computed using the following formula:

$$\rho \frac{\partial u}{\partial t} + \rho u \cdot \nabla(u) = -\nabla p + \nabla \cdot \tau - \rho \beta (T - T_{ref}) g \tag{2}$$

where p and β denote the fluid pressure (Pa) and coefficient of thermal expansion (K^{-1}), respectively. τ describes the vector of stress tensor (kg·m^{-1}·s^{-1}).

The conservation of mass is given by:

$$\frac{\partial \rho}{\partial t} = \nabla \cdot (\rho u) \tag{3}$$

The energy equations are applied to all layers of PV module and heat storage tank. The glass surface of the PV module experiences both convection and radiation. The PV module's upper and bottom sides have equivalent convection heat transfer coefficients, which are dictated by wind speed. The internal heating source part in the energy conservation equation for the glass and cells is computed using Eqs. (4) and (5) [40], respectively. In addition, before reaching the PV cell, the energy strikes the PV module and goes through the glass and EVA layer. The quantity of energy that reaches the cells is determined by the absorptivity and transmissivity of the layers above it, as well as the incidence angle. Therefore, the cell's zero transmissivity resulted in no heat generation in the layers underneath it.

The thermal energy source in the glass layer can be expressed as below:

$$\dot{Q}_g = \frac{\alpha_g G}{\delta_g} \tag{4}$$

The thermal energy source in the PV layer is calculated as below:

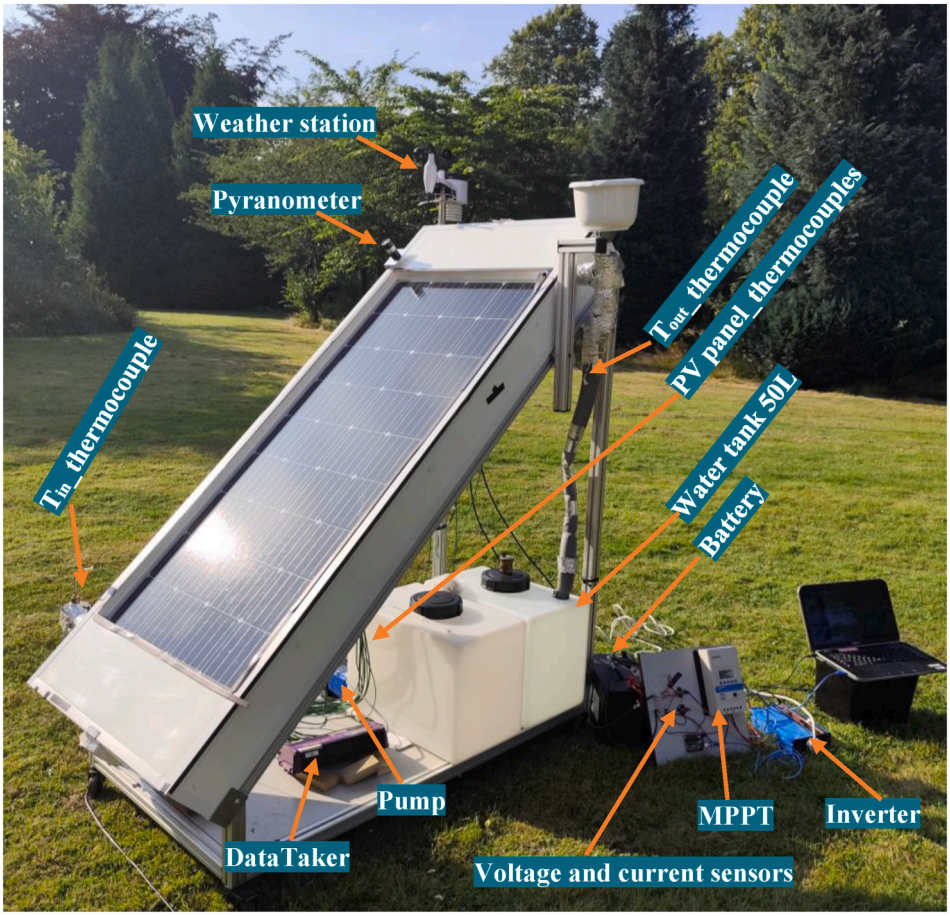

Fig. 2. Experimental set-up of closed-loop hydronic cooling of PV panel.

$$\dot{Q}_{PV} = \frac{(\tau\alpha)_{PV} G - \xi P_{elec}}{\delta_{PV}} \tag{5}$$

where δ_g and δ_{PV} represent the thickness of glass cover layer and PV layer, respectively; G and ξ are solar irradiation on the top surface of PV module (W/m^2) and packing factor; P_{elec} is electrical energy (W/m^2) [17].

$$P_{elec} = G\tau_g\eta_{ref}\left[1 - \beta_{ref}\left(T_{PV} - T_{ref}\right)\right] \tag{6}$$

where τ_g and T_{PV} represent the glass cover transmissivity and the PV plate temperature, respectively. η_{ref} describes the PV cell's referenced efficiency at a reference temperature T_{ref}, and β_{ref} is the thermal coefficient of PV cell, which is equal to 0.0045/K [18]. The effective transmissivity-absorptivity for PV layer is described as follows [19]:

$$(\tau\alpha)_{PV} = \frac{\tau_g\alpha_{PV}}{1 - (1 - \alpha_{PV})r_g} \tag{7}$$

where r_g and α_{PV} denote the glass layer reflectivity and PV cell's absorptivity, respectively.

Regarding the similar system specification [20], it has been calculated that 0.5 W/m^2 of pump power is required. Consequently, the net power production from the proposed PV module system is expressed as below:

$$P_{net} = P_{elec} - P_{pump} \tag{8}$$

3.2. Numerical procedure

The numerical procedure adopted in this work is illustrated in the flowchart shown in Fig. 3. Computing techniques often use iterative schemes to produce simulated results. These iterations commonly get carried out over time and need particular criteria to figure out convergence. The current numerical simulation establishes the convergence criteria at a relative tolerance of 10^{-4}, or 0.01 %, which is substantially within the reasonable range. For instance, the PV layer's internal heat source term is calculated using an iterative technique. The initial round of iteration assumes a PV efficiency of 15 %, and the governing equations are solved to calculate the average PV layer temperature. This increased average temperature is then used in Eq. (6) to compute the photoelectric efficiency of conversion. According to the estimated efficiency, the term of heat generation in the PV layer is altered for the subsequent iteration. The operation is continued until the difference in average PV temperature between iterations is less than 0.01 %. COMSOL Multiphysics, a commercial package using the finite element method (FEM), is applied to solve heat transfer and fluid flow problems. The partial differential equations (PDEs) are transformed into algebraic equations through discretization to solve them. The model's equations are entirely nonlinear and fully coupled. As a result, these equations are solved at the same time until the convergence conditions are achieved - the residuals for all variables.

Whenever the temperature distribution is determined, the PV efficiency, power output, and other necessary calculations are performed. The cooling energy for the PV module during nighttime can be determined by the change in thermal energy of water flow, which is written below [21,22]:

$$E_{th} = \frac{\dot{m}C_{p,w}(T_{in} - T_{out})}{A_p} \tag{9}$$

where E_{th} is the heat transfer or cooling energy absorbed by the water

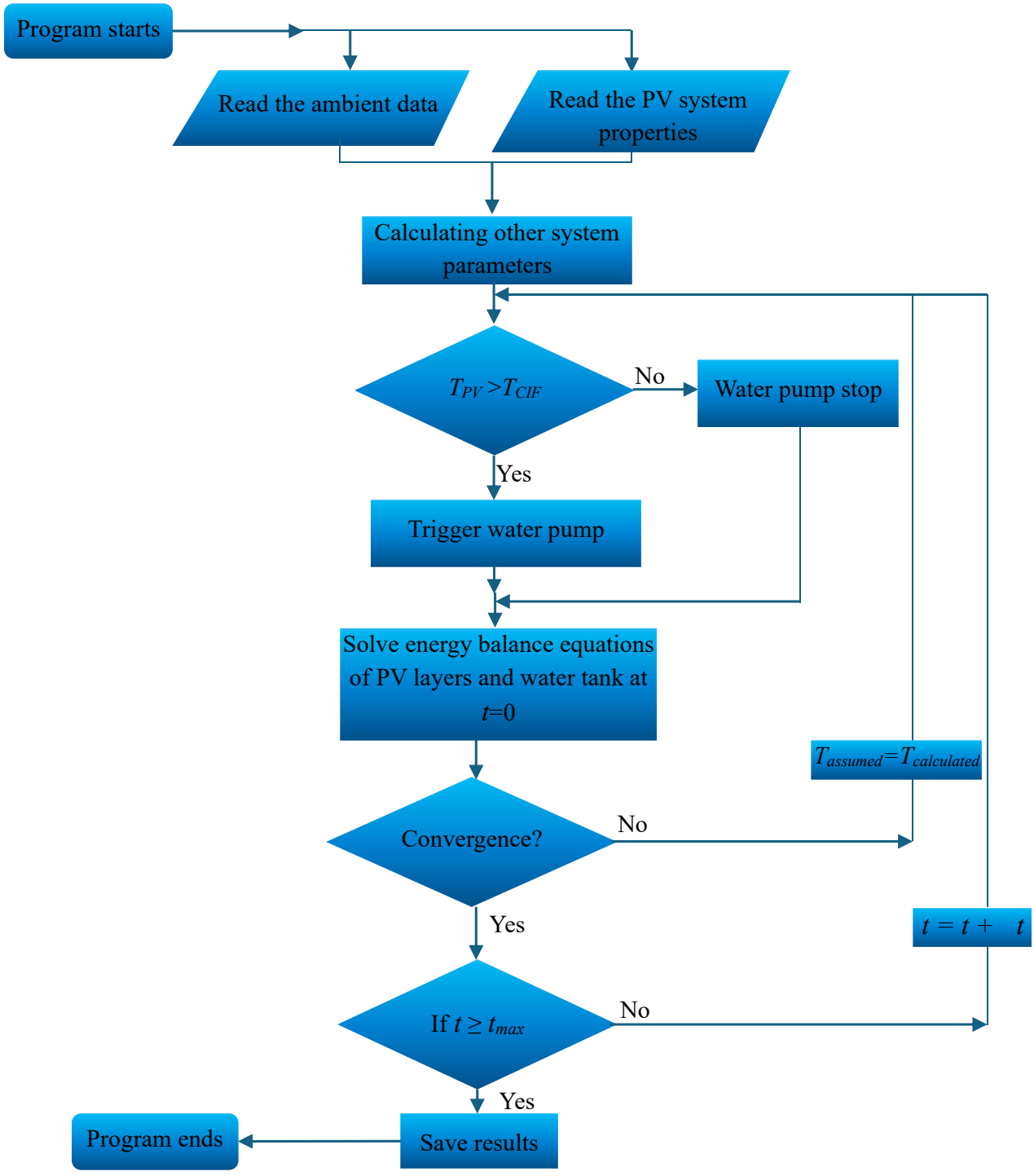

Fig. 3. Flowchart of the simulation procedure.

within copper tubes during the testing or simulation periods (W/m^2). A_p is the panel area (m^2), while $\dot{m}$ is the water flow rate (kg/s) inside the manifold. T_{in} and T_{out} are the inlet and outlet water temperatures, respectively.

3.3. Boundary conditions

A 3D time-dependent numerical model has been developed in this simulation using the COMSOL programme to calculate the cooling and electrical performance of PV module and heat storage tank. To address the general governing equations described in previous Section 3.1 related to the various layers of PV panel, storage tank and water tubes, the boundary condition for each element within the whole unit have been set as below [23,24].

1. At the upper surface of the glass cover, the radiation heat transfer is calculated by:

$$q_{sky,g} = \varepsilon_g k_B \left(T_{sky}^4 - T_g^4 \right) \tag{10}$$

where ε_g is the glass cover emissivity, T_g represents the temperature of the glass cover. k_B denotes Stefan Boltzmann constant, equal to 5.67 × 10^{-8} (W m^{-2} K^{-4}) and T_{sky} denotes the temperature of sky, which is related to the temperature of ambient (T_a) [25]:

$$T_{sky} = 0.0522 T_a^{1.5} \tag{11}$$

2. At the exterior boundary surfaces, convective heat transfer:

$$q_{a,g} = h_a (T_a - T_{ext}) \tag{12}$$

where T_{ext} represents the temperature of exterior (outer) surfaces to ambient such as glass, tubes, aluminium absorber plate and water tank. H_a is the exterior convective heat transfer coefficient, and it is given based on the wind velocity (u_a) as described in Ref. [26]:

$$h_a = 2.8 + 3.0 u_a \tag{13}$$

3. The edges of PV module are assumed to be adiabatic:

$$\frac{\partial T_s}{\partial n} = 0 \tag{14}$$

where n indicates the normal distance of the surface along the x, y, or z axes, accordingly. In addition, the water leaving the PV panel manifold is directed into the storage tank, whilst the water from this tank subsequently circulates back into the manifold of PV panel as inlet.

3.4. Degradation rates and failure time models

The degradation rate model represents a mathematical function that determines how stress variables affect performance degradation. The modified model by Ref. [27] could be implemented for estimating outdoor degradation. Individual rate models were combined to create a comprehensive rate of degradation model, as outlined below:

$$K_T = A_N \cdot (1 + k_H)(1 + k_P)(1 + k_{Tm}) - 1 \tag{15}$$

where K_T ($year^{-1}$) denotes the total degradation rate, while A_N ($year^{-2}$) is the constant utilized for normalizing the physical quantity. The degradation rate of hydrolysis, thermomechanical process and photodegradation are described by k_H, k_{Tm} and k_P ($year^{-1}$), respectively. The degradation rates due to specific processes were evaluated with respect to environmental stress as below:

$$k_H = A_h \cdot RH^n \cdot \exp\left(-\frac{E_{ah}}{k_B T_{\mathrm{mod}}} \right) \tag{16}$$

$$k_P = A_p \cdot UV^X (1 + RH^n) \cdot \exp\left(-\frac{E_{ap}}{k_B T_{\mathrm{mod}}} \right) \tag{17}$$

$$k_{Tm} = A_t \cdot C_N \cdot (273.15 + \Delta T)^{\theta} \cdot \exp\left(-\frac{E_{at}}{k_B T_{\max}} \right) \tag{18}$$

where A_h ($year^{-1}$), A_p ($m^2 \cdot kWh^{-1}$) and A_t ($°C^{-1} cycle^{-1}$) are the pre-exponential constant associated with hydrolysis, photodegradation as well as thermomechanical processes, respectively. E_{ah}, E_{ap} and E_{at} (eV) represent the activation energies of power degradation. T_{mod} (K) describes the mean PV panel temperature, X and n describe the model factors that show the impact of UV solar irradiation dosage ($kW \cdot a^{-1} \cdot m^{-2}$) and the relative humidity rate on the power degradations. $\Delta T = (T_{max} - T_{min})$ represents the temperature variation, $T_{\max}$ and $T_{\min}$ represent the temperature of the PV maximum and minimum, C_N is the cycling rates, ($cycles \cdot year^{-1}$).

The degradation rate evaluation is used to estimate the lifetime of PV panel, with the failure time (t_f) described as follows [28]:

$$t_f = \frac{\Gamma}{K_T \cdot (|\ln(0.2)|)^{\mu^{-1}}} \tag{19}$$

where μ is the shape factor and Γ denotes the factor associated with the materials. The extracted factors used to evaluate the annual degradation rate and lifespan are shown in Table 2.

3.5. Mesh analysis

The equations, boundary and initial conditions have been integrated and solved using the finite elements analysis software COMSOL Multiphysics, and the fine mesh is chosen after taking grid independence testing. To verify the independence of the mesh, simulations were carried out with different numbers of elements (193,705, 476,569, 544,407, and 621,810) on the PV Module results. The findings, as depicted in Fig. 4, showed a small difference, thus validating the mesh independence. This mesh independence study was conducted over two days in July (the 16th and 17th) to observe variations under different times and weather conditions. Hence, a grid comprising 544,407 elements was employed in the simulation conducted for the parametric study. Fig. 5 depicts the meshing of the computational domain for the PV module system, utilizing the provided physics-controlled meshing features.

4. Results and discussion

The thermal and electrical performance of the proposed PV system over 24 h was numerically investigated according to mathematical modellings in comparison with a common PV panel. In addition, the influence of several key factors such as control flow on PV performance was analysed. The weather data for the simulation were sourced via standard meteorological year data for Basra in Iraq and used for the parametric evaluation process. This data was obtained from the EnergyPlus™ weather data website [29].

4.1. Validation of the simulation using experimental data

The build mathematical model accuracy verified using comparing it to experimental data gathered before it is used to estimate the performance of the closed-loop PV system for different scenarios. In the present study, the Mean Relative Error (MRE) was employed to assess the precision of the model concerning specific essential variables. The equation of MRE was utilized to measure the disparity between the simulation outcomes and the experimental data for the purpose of evaluating the accuracy of the model [30]:

$$MRE = \frac{1}{N} \sum_{i=1}^{i=N} \left| \frac{X_{\exp} - X_{sim}}{X_{\exp}} \right|_i * 100\% \tag{20}$$

where $X_{\exp}$ refers to the experimental findings, while X_{sim} denotes the outcomes of the simulation.

As previously stated, experimental data collected on June 2, 2024, is employed to verify the accuracy of the mathematical model. The comparison between simulated and experimental values is illustrated in Fig. 6(a), (b) and (c). Fig. 6(a) shows the simulated and experimental results for the inlet and outlet water manifold temperatures. The results reveal a strong agreement between simulated and experimental data over the testing period. The MRE of these inlet and outlet temperatures in the manifold were 3.1 % and 2.2 % respectively. Fig. 6(b) demonstrates that the experimental and simulated temperatures in the water tank were highly consistent. The measured and predicted temperatures of the water tank over the testing period had a MRE of 5.7 %.

Table 2
Parameter values utilized in degradation rates and lifetime models [28].

Factor	A_h	A_p	A_t	E_{ah}	E_{ap}	E_{at}	n	X	Θ	Γ	μ
	$year^{-1}$	$m^2{\cdot}kWh^{-1}$	$^{\circ}C^{-1}cycle^{-1}$	eV	eV	eV					
Values	4.34×10^7	43.95	2.45	0.83	0.51	0.46	1.72	0.63	1.8	1.2	0.3

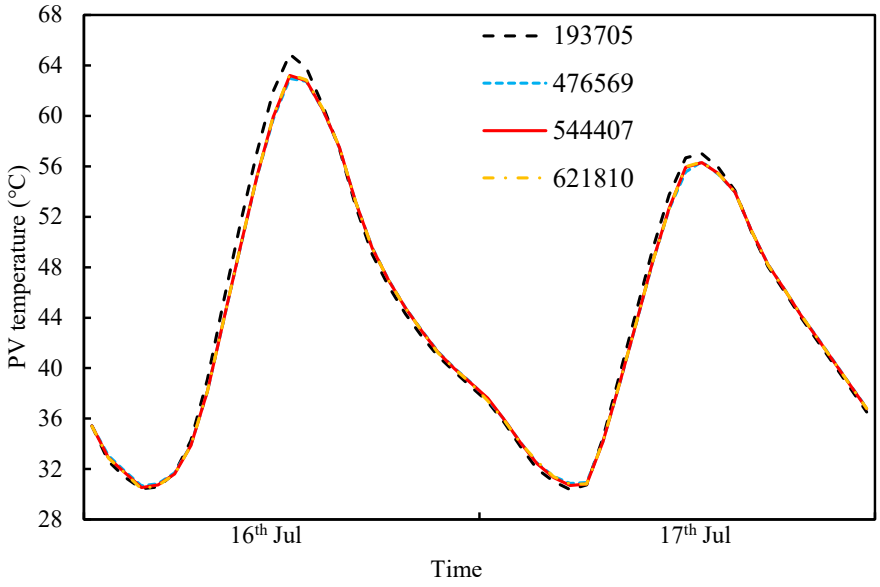

Fig. 4. The PV panel temperature against the number of mesh elements.

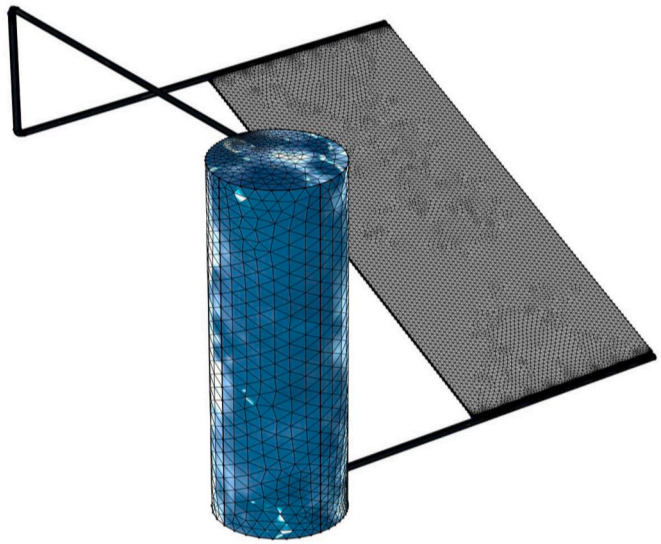

Fig. 5. The Meshing Generation for the PV cooling system.

In addition, from Fig. 6(c), the experimental electrical output is slightly higher than the simulated result in the beginning and final testing stages. The MRE value of electrical outpower was only 6.8 %. This discrepancy between the experimental setup and the simulation results can be explained by variations in the initial boundary conditions and the thermal inertia of the frame and insulation of the PV module components [5,31]. The unknown initial temperatures of the experimental components greatly influenced the initial simulation outcomes, particularly in cases involving transient behaviour.

4.2. Seasonal analysis of the controlled intermittent flow (CIF) in the closed-loop hydronic cooling of PV panel

The simulated results of the proposed closed-loop hydronic cooling of PV panel with controlled intermittent flow (CIF), continuous flow (CF), and common PV (Com) are compared and analysed in this section, using a set PV temperature value (T_{CIF}) of 35 °C for CIF during both daytime and nighttime in winter and summer. To figure out the characteristics of the proposed PV system, hourly heat patterns have been investigated. Fig. 7 demonstrates the PV panel's hourly rate of heat transfer and ambient temperature during five consecutive days across winter (January 16th to 20th) and summer (July 16th to 20th). As illustrated in Fig. 7(a) and (b), both pump working hours and T_{PV} of the common and proposed systems (CIF and CF) in winter and summer, respectively. It can be observed that the proposed system with CIF reduced temperature fluctuation compared to common PV, as well as decreased pump consumption by reducing the pump's operating hours when T_{CIF} equals 35 °C, especially in winter compared to summer. In fact, the closed-loop PV system can maintain the T_{PV} below 36 °C in winter and 60 °C in summer.

On the other hand, Fig. 8 compares the daily total net output power of the three systems. Interestingly, the net output power difference between the CIF system and the other two systems is larger in winter. The seasonal P_{net} enhancement for the CIF system is predicted to be 0.57 % and 0.83 % for winter and summer, respectively compared to the CF system. The net power enhancement in winter is the biggest, mainly due to the lower pump working hours and T_{PV}.

4.3. Annual analysis of the controlled intermittent flow (CIF) in the closed-loop hydronic cooling of PV panel

4.3.1. Effect on PV performance

The effects of the proposed systems over a whole year are

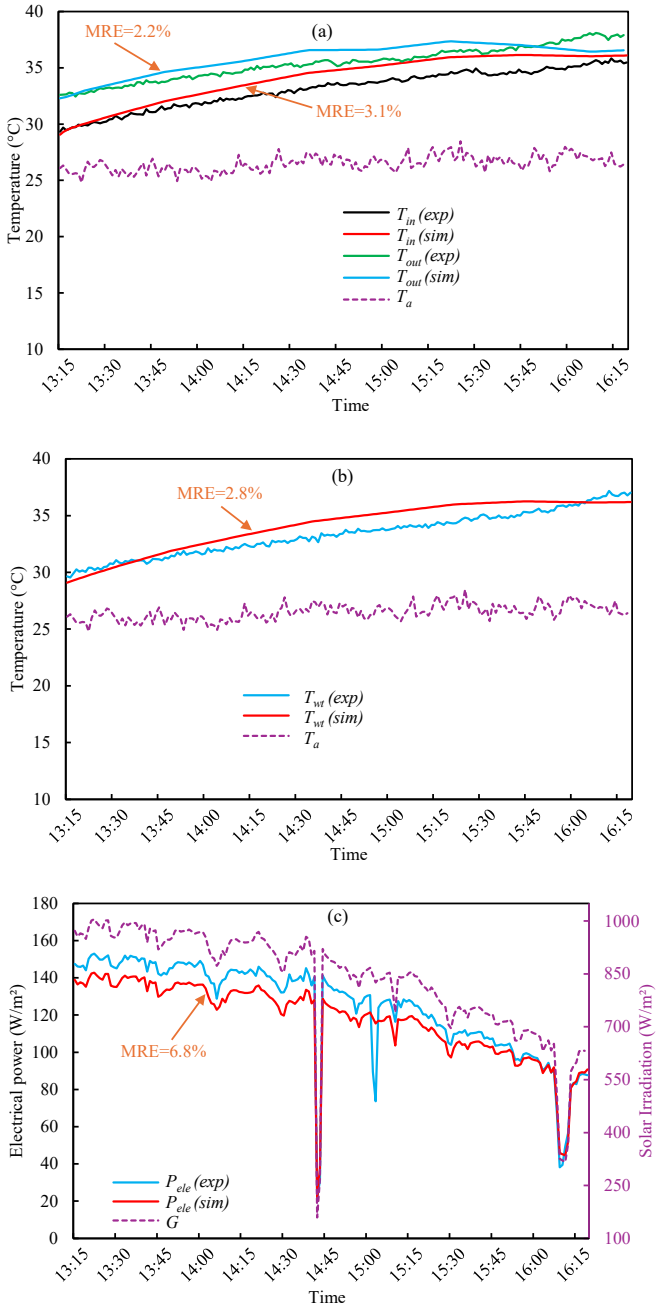

Fig. 6. Experimental and simulated (a) temperature of water at the inlet and outlet of the manifold (b) temperatures of the water storage tank (c) electrical power.

investigated in Fig. 9 by changing the system from CF to CIF with T_{CIF} = 25 °C, 35 °C and 45 °C and compared to common PV. It can be seen from Fig. 9(a) that the T_{PV} is lower year-round with CF. The pump working hours are the lowest during winter and nighttime, which leads to decreased operating time in the CIF system compared to the CF system. The monthly total of P_{net} of the proposed systems with CIF, CF, and common PV is presented in Fig. 9(b). In overall months, the monthly total of P_{net} increases with the use of the CIF system with T_{CIF} = 35 °C by 0.96 % compared to the CF system due to the reduced pump consumption power resulting from decreased working hours, as noted in Fig. 9(a).

Furthermore, the water tank temperature at peak times is lower when the set point temperature (T_{CIF}) is higher because this reduces the water circulation in the PV system, which helps maintain a lower water tank temperature, as shown in Fig. 10(a). This can lead to a decrease in the maximum T_{PV} and provide a better temperature when needed according to the T_{CIF} value. Moreover, this results in reduced pump operating hours, as illustrated in Fig. 10(b). Hence, the pump operating time should be optimized according to the preferred or required PV operating temperature.

Finally, seasonal adjustments to set temperatures can significantly improve system performance and energy efficiency. Lower set PV temperatures (like T_{CIF} = 25 °C) are recommended during winter months (November, December, and January) to maximise net power, enabling the system to operate more effectively under cooler conditions as shown in Fig. 9(b). Conversely, higher set temperatures (e.g., T_{CIF} = 35 °C) are more effective for power saving during warmer months, such as May through October. This adjustable controlled cooling strategy ensures optimal CIF system performance throughout the year, promoting efficient cooling technique and reducing pump working hours.

4.4. Effect of climate conditions

In this section, we analyse the differences in performance, degradation rates, and lifetime estimates across various locations, Basra in Iraq (30.55° N, 47.67° E), Nottingham in UK (52.95° N, 1.16° W) and Hong Kong in China (22.25° N, 113.85° E). These urban areas are located in the Hot-Dry, Cold-Humid, and Warm-Humid climate zones, respectively.

4.4.1. Effect on performance

Fig. 11 compares the annual total of P_{net} for the CIF system at a set point of T_{CIF} = 35 °C with the CF system and the common PV system across the three previously mentioned locations. In all locations, regardless of climate zone, the annual total of P_{net} is higher for the CIF system than for the other systems. This increase is particularly notable in regions with elevated ambient temperatures, such as Hong Kong in China and Basra in Iraq.

In Iraq, the CIF system exhibits a 0.96 % improvement over the CF system and a 2.23 % enhancement over the common PV system. In Hong Kong, the CIF system shows a relatively slight improvement of 2.07 % over the CF system, while the P_{net} value of the CIF system exceeds that of the common PV system by 1.07 %. Conversely, in regions with cold and humid climates like the UK, the CF PV module may perform worse than the common PV system. Specifically, the overall annual P_{net} in the UK decreases by 1.95 % when using the CF system compared to the common PV system. However, with the CIF system, there is a 0.67 % improvement over the common PV system and a 2.69 % increase compared to the CF system. This is due to the shorter duration of pump operation in cold climates, which leads to reduced pump power consumption when the PV module temperature is lower than the set point (T_{CIF}).

4.4.2. Effect on degradation rate and lifespan

This study employs degradation rates to forecast the lifetime of a particular PV module. equations (15)–(19) are used to calculate the Mono-cSi 150 W PV module's total degradation rates and failure time. The model offered in Ref. [27] is applied for calculating the average yearly degradation rates for different PV panels, with the different climate changes in Iraq, UK and China. The acquired factors are taken from Ref. [27] and the calculated climate variables for three different climates are derived from the area of measurement and PV parameters (Table 3).

The observed data were contrasted with results from models expecting degradation rates in a neighbouring location near Basra, which showed consistent findings as outlined in these cited studies [27,28,32]. The proposed CIF closed-loop hydronic cooling of PV panel has a lower maximum operating temperature, which is up to 8.75 °C lower in Iraq compared to the common system. This reduction in temperature decreases the degradation rate and increases the PV module's lifetime,

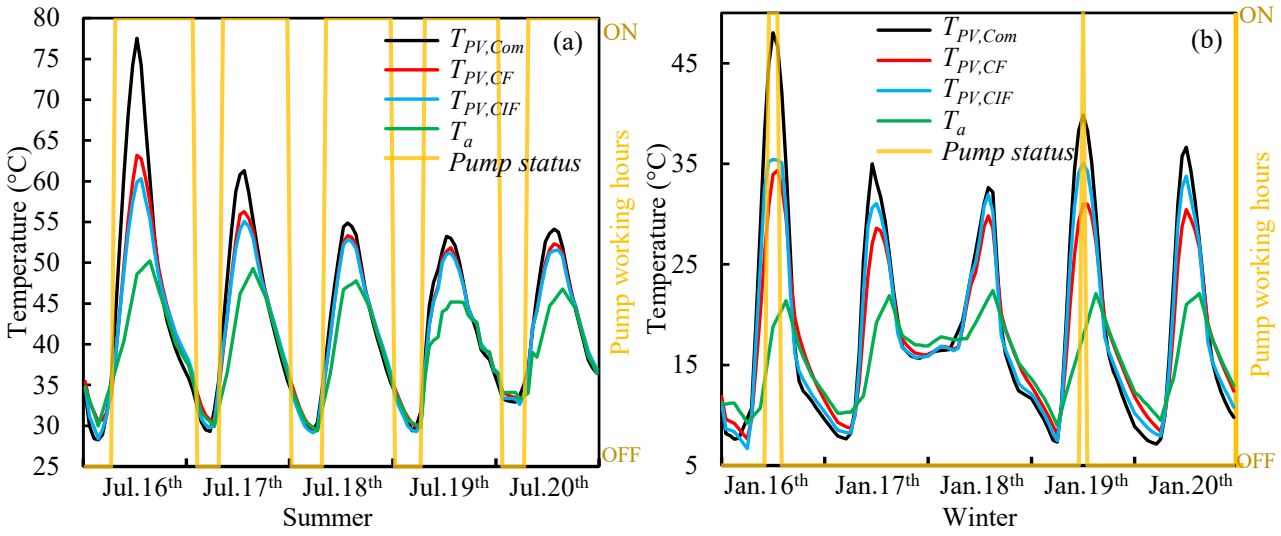

Fig. 7. The PV temperature comparison with the common and proposed system CIF and CF, during (a) winter and (b) summer in Basra.

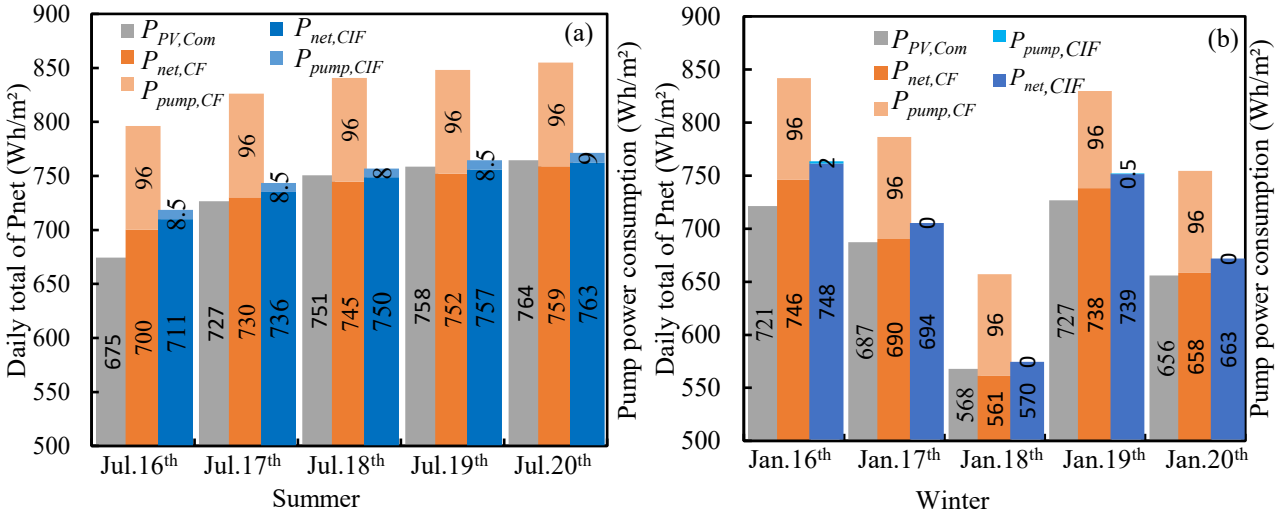

Fig. 8. Comparative analysis of PV performance between the common and proposed systems, considering CIF and CF, under (a) summer and (b) winter conditions in Basra.

as illustrated in Fig. 12. It was found that both CF and CIF systems have a considerable improvement in lifetime of up to 34.3 % and 41 % over common PV (Com) systems, respectively as seen in Fig. 12(b). Moreover, the CIF system shows a significant improvement compared to the other two systems, with enhancements of 4.9 % and 22.2 % over the CF and common PV systems, respectively. These data imply that employing the proposed CF or CIF in this system improves heat management, potentially increasing PV panel efficiency and lifespan. In contrast, findings in the UK indicate that CF cooling systems are expected to have a longer lifespan compared to other PV systems. However, a drawback of CF systems is their high pump operating hours, leading to a decrease in net power production. Consequently, it may be beneficial to optimize the working hours of CIF systems to coincide with the hottest months/time and locations, thereby reducing the maximum temperature of PV systems. This adjustment is considered crucial in mitigating the degradation rates and increasing the lifespan of PV systems.

These findings indicate that the implementation of the proposed CIF cooling system within photovoltaic (PV) systems has the potential to markedly enhance thermal regulation in regions characterized by elevated temperatures and aridity. This methodology may facilitate improved water conservation and a diminished degradation rate, ultimately culminating in a prolonged operational lifespan for the system. Previous research [33] indicates that the application of spray water cooling in Al Sharjah typically results in an annual degradation rate of approximately 1.214 % over a lifespan of 19.8 years, which is comparatively greater than that associated with the proposed CIF system. Ahmad et al. [34] conducted an empirical investigation that revealed the utilization of water mist or fog to cool the underside of a PV panel led to a reduction in degradation rates by 0.8 % annually, thereby extending the operational lifespan of the panel to 30 years. While their results highlight the potential of enhanced cooling strategies, the excessive water consumption, high maintenance requirement, and significant evaporation loss of such open-loop systems limit their practicality in hot and arid regions. In this context, the CIF system, with its efficiency and minimal water usage, might be a more sustainable choice for these areas.

4.4.3. *Application potential*

In this section, we examine the practical consequences of the CIF

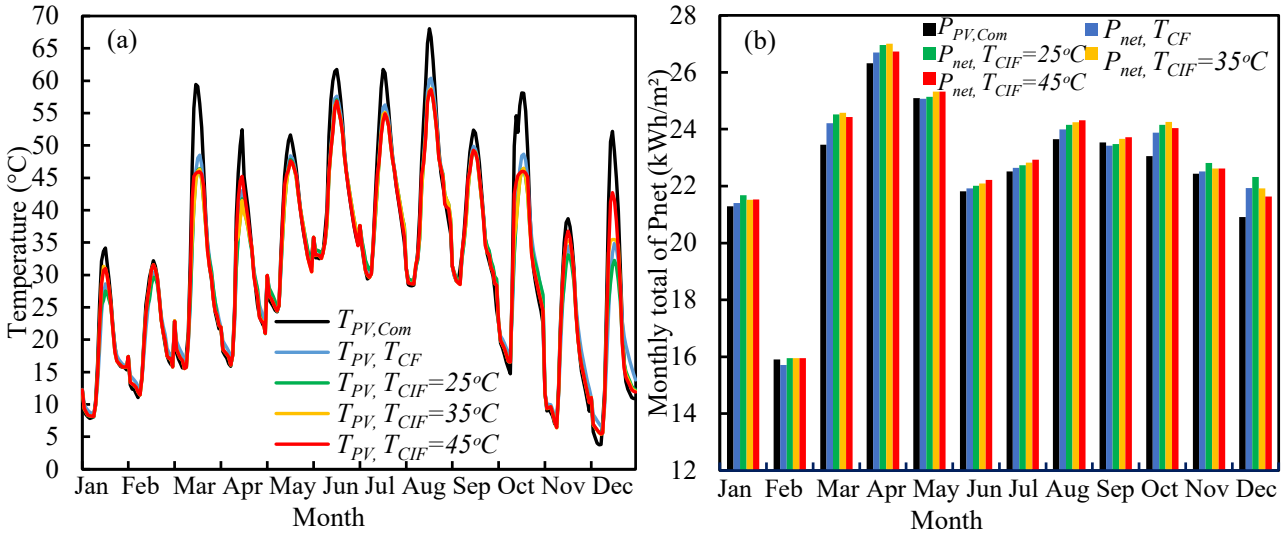

Fig. 9. Comparison of PV performance between the common, CF, and CIF systems: (a) hourly values of T_{PV} for a typical day in each month and (b) monthly total of P_{net}.

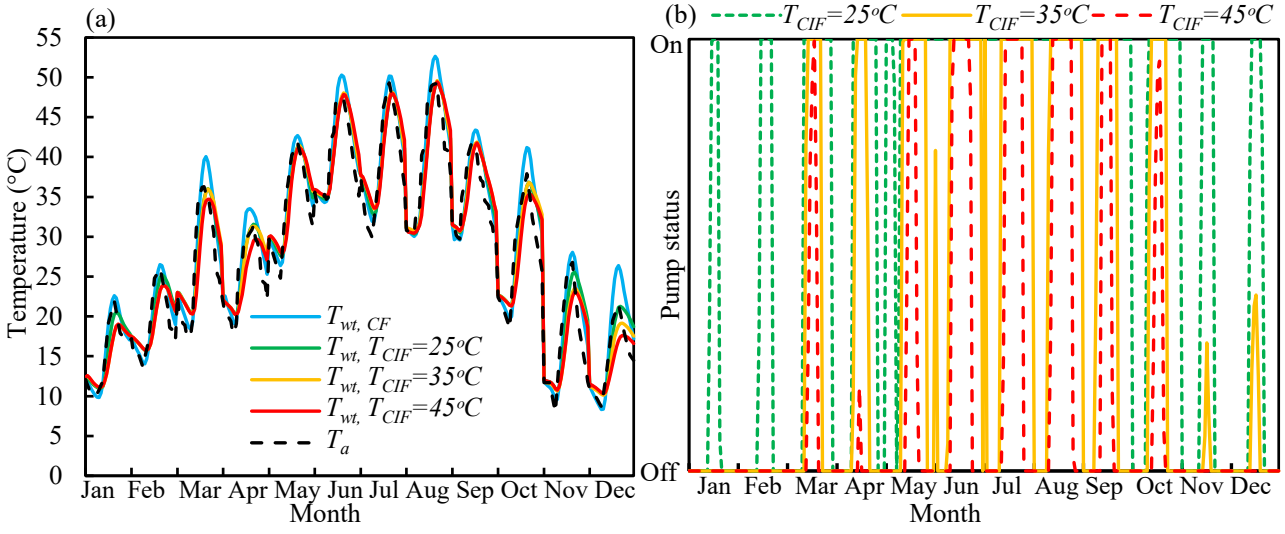

Fig. 10. Effect of different set points (T_{CIF}) on (a) temperature of water tank (T_{wt}) and (b) pump status for a typical day in each month.

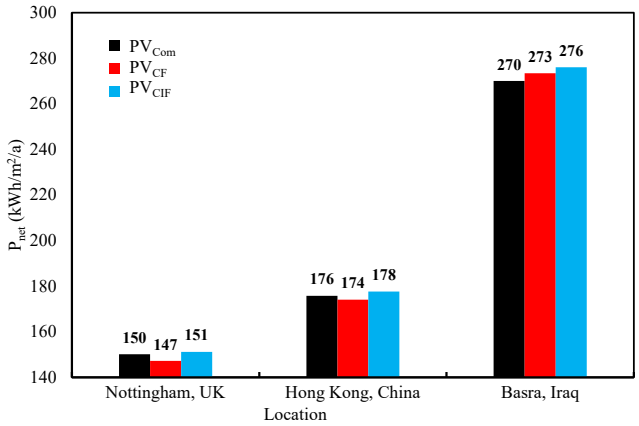

Fig. 11. Comparison of the total annual P_{net} for the proposed CIF, CF and common PV systems in Nottingham, Hong Kong and Basra.

Table 3
The measured annual environmental variables and PV panel data for the three locations are used to determine degradation rates and lifespan.

City, Country	PV Modules	T_{mod} °C	T_{max} °C	T_{min} °C	RH %	UV dose kWh/a/m^2
Basra, Iraq	Com	31.88	65.78	4.1	61.5	96.7
	CF	30.6	58.5	7.1	61.5	96.7
	CIF	30.47	57	5.7	61.5	96.7
Nottingham, UK	Com	11.99	33.9	−2	78	55
	CF	11.75	31	0.53	78	55
	CIF	11.75	31.9	−0.3	78	55
Hong Kong, China	Com	25.1	48	10.5	75	90.75
	CF	25.05	43	11.2	75	90.75
	CIF	24.89	41.3	10.8	75	90.75

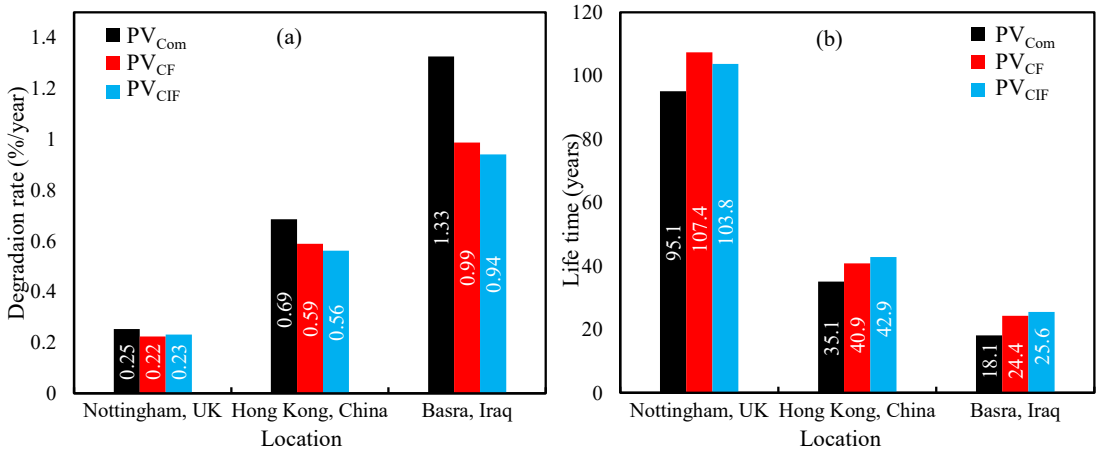

Fig. 12. Comparison of degradation rates and failure times among CF, CIF and common PV systems.

system's 0.96 % reduction in pump energy use. CIF decreases energy consumption by pump and inefficiency in operation in large-scale solar PV systems, resulting in increased system performance and energy savings. Over long durations of operation, this decrease can result in cumulative energy savings of around 3 kWh per year per unit, contributing to cost reductions, particularly in large-scale or energy-intensive applications. After a preliminary calculation, the payback period for the CIF system is estimated to be approximately 6–7 years. While it slightly increases the initial system cost, it maintains strong economic performance, comparable to that of common PV systems.

Furthermore, by reducing energy demand, the CIF system reduces the environmental load by lowering carbon emissions, which helps to achieve sustainability goals. The suggested CIF system not only improves energy efficiency, but also offers significant water savings, particularly in arid regions where water scarcity is critical. Its closed-loop design is more sustainable than traditional open-loop systems, which experience significant evaporation losses. The CIF system offers significant water savings, making it ideal for hot and arid regions facing water scarcity. It circulates only 150 L of water, compared to approximately 189 L/h or about 551,880 L/year for an open-loop cooling system [35]. This represents an annual water savings of over 99.97 %, highlighting the environmental benefits of adopting a CIF system over traditional open-loop systems. Furthermore, the CIF system decreases the danger of long-term damage by minimising mechanical stress, making it a durable and cost-effective solution for varying operational conditions.

5. Conclusions

In this research, a closed-loop hydronic controlled intermittent flow (CIF) and continuous flow (CF) cooling for a PV system is proposed with controlled flow conditions to optimize both power production and cold energy harvesting. The primary operational concept involves utilizing the PV panel as a cooling surface during nighttime, allowing cold energy to be harvested by circulating water beneath it in a closed-loop circuit. During the day, the stored cold water is pumped into the water channel to cool the PV system. A 3D transient thermal model was developed and COMSOL simulations were used to assess the net generated power of the proposed PV system. The conclusions drawn from the simulation results are as follows.

1. The proposed PV cooling system with CIF lowers seasonal fluctuation in temperature and pump power demand by reducing running hours, particularly in the winter. Compared to common PV, this proposed system can keep PV temperature below 36 °C in winter and 60 °C in summer at $T_{CIF} = 35$ °C.
2. The predicted seasonal net power enhancement for the CIF system is 0.57 % and 0.83 % for winter and summer, respectively, compared to the CF system.
3. The monthly total of net power in Iraq consistently rises by 0.96 % throughout all months when employing the CIF system with $T_{CIF} = 35$ °C in contrast to the CF method. This rise is related to the lower power consumption of the pump, which occurs as a result of reduced duration of operation.
4. It has been found that both CF and CIF systems for Iraq have a considerable improvement in lifetime of up to 34.3 % and 41 % over common PV system, respectively. Furthermore, in Hong Kong, the CIF system demonstrates a notable improvement, outperforming the CF and common PV systems by 4.9 % and 22.2 %, respectively.

The simulation results offer important insights regarding the operational performance of the proposed PV CIF system, highlighting its advantages in reducing pump power demand and increasing net power output. Furthermore, the effect of the CIF set PV temperature value on the pump working hours related to PV temperature was also elucidated, providing crucial design considerations for future developments in this field. A limitation of this study is that the CIF system has not yet been tested in Iraq, nor has the measured data been validated using simulation models. In the future, we will conduct experimental validation in Iraq and apply the proposed CIF system to large-scale PV systems.

CRediT authorship contribution statement

Hazim Dirawi: Writing – review & editing, Writing – original draft, Visualization, Validation, Software, Methodology, Investigation, Formal analysis, Data curation, Conceptualization. **Qiliang Wang:** Writing – review & editing, Writing – original draft, Supervision, Methodology, Investigation, Formal analysis. **Mingke Hu:** Software, Formal analysis. **Yuehong Su:** Writing – review & editing, Writing – original draft, Supervision, Resources, Project administration, Methodology, Funding acquisition, Formal analysis, Conceptualization. **Saffa Riffat:** Supervision, Resources, Project administration.

Declaration of competing interest

The authors declare that they have no known competing financial interests or personal relationships that could have appeared to influence the work reported in this paper.

Acknowledgement

The authors wish to thank the Higher Committee of Education

Development in Iraq (HCED) for providing financial support for the PhD scholarship that facilitated this research endeavour. The authors would also like to thank the Engineering and Physical Sciences Research Council for funding support to the Marie Sklodowska-Curie fellowship (Horizon Europe Guarantee grant number: EP/Y016645/1).

Nomenclature

A	area, m^2
C_p	specific heat capacity, $J{\cdot}kg^{-1}{\cdot}K^{-1}$
d	diameter, m
E	energy, $W{\cdot}m^{-2}$
E_a	activation energy, eV
g	acceleration of gravity, $m{\cdot}s^{-2}$
G	solar radiance, $W{\cdot}m^{-2}$
h	heat transfer coefficient, $W{\cdot}m^{-2}{\cdot}K^{-1}$
k	degradation rates, $year^{-1}$ or thermal conductivity, $W{\cdot}m^{-1}{\cdot}K^{-1}$
k_B	the Stefan Boltzmann factor, $W{\cdot}m^{-2}{\cdot}K^{-4}$
L	litre, L
$\dot{m}$	mass flow rate, $kg{\cdot}s^{-1}$
P	Power, $W{\cdot}m^{-2}$
PV	photovoltaic
$\dot{Q}$	energy generation rate, $W{\cdot}m^{-3}$
t	time, s
t_f	failure time, years
T	temperature, K
u	wind or fluid velocity, $m{\cdot}s^{-1}$

Greek symbols

τ	stress tensor, $kg{\cdot}m^{-1}{\cdot}s^{-1}$ or transmissivity, –
$(\tau\alpha)$	transmittance–absorptance, –
α	absorptivity
δ	layer thickness, m
β	thermal expansion constant, K^{-1}
ε	emissivity, –
ρ	density, $kg{\cdot}m^{-3}$
ξ	packing factor, –
η	efficiency, –

Abbreviations

ΔT	the temperature variance, K
a	annual
CF	continuous flow
CIF	controlled intermittent flow
Com	common PV
exp	experimental data
EVA	Ethylene Vinyl Acetate
in	inlet
out	outlet
p	panel
rad	solar radiation
sim	simulation data

subscript

a	ambient
g	glass
fc	cross-sectional flow
elec	electrical
ref	reference
w	water
wt	water tank

References

[1] Y.F. Nassar, A.A. Salem, The reliability of the photovoltaic utilization in southern cities of Libya, Desalination 209 (2007) 86–90, https://doi.org/10.1016/J.DESAL.2007.04.013.

[2] S. Heo, D.H. Kim, Y.M. Song, G.J. Lee, Determining the effectiveness of radiative cooler-integrated solar cells, Adv. Energy Mater. 12 (2022) n/a, https://doi.org/10.1002/aenm.202103258.

[3] C. Peike, S. Hoffmann, P. Hülsmann, B. Thaidigsmann, K.A. Weiβ, M. Koehl, et al., Origin of damp-heat induced cell degradation, Sol. Energy Mater. Sol. Cell. 116 (2013) 49–54, https://doi.org/10.1016/j.solmat.2013.03.022.

[4] R. Laronde, A. Charki, D. Bigaud, Lifetime estimation of a photovoltaic module subjected to corrosion due to damp heat testing, J. Sol. Energy Eng. 135 (2013), https://doi.org/10.1115/1.4023101.

[5] H. Dirawi, Q. Wang, M. Hu, Y. Su, S. Riffat, A hydronic closed-loop photovoltaic cooling system designed for hot and arid regions: performance evaluation and degradation rate/lifetime analysis, Appl. Energy 373 (2024) 123999, https://doi.org/10.1016/J.APENERGY.2024.123999.

[6] D. Weber, M.I.R. Jani, M. Grabo, O. Wallscheid, J. Böcker, T. Klaus, et al., Lifetime extension of photovoltaic modules by influencing the module temperature using phase change material. 2018 IEEE 7th World Conference on Photovoltaic Energy Conversion (WCPEC) (A Joint Conference of 45th IEEE PVSC, 28th PVSEC & 34th EU PVSEC), 2018, pp. 784–789, https://doi.org/10.1109/PVSC.2018.8548115.

[7] R. Tripathi, G.N. Tiwari, Energy matrices, life cycle cost, carbon mitigation and credits of open-loop N concentrated photovoltaic thermal (CPVT) collector at cold climate in India: a comparative study, Sol. Energy 186 (2019) 347–359, https://doi.org/10.1016/J.SOLENER.2019.05.023.

[8] S. Abo-Elfadl, S. Yousef M, M.F. El-Dosoky, H. Hassan, Energy, exergy, and economic analysis of tubular solar air heater with porous material: an experimental study, Appl. Therm. Eng. 196 (2021) 117294, https://doi.org/10.1016/J.APPLTHERMALENG.2021.117294.

[9] M. Rezvanpour, D. Borooghani, F. Torabi, M. Pazoki, Using CaCl2·6H2O as a phase change material for thermo-regulation and enhancing photovoltaic panels' conversion efficiency: experimental study and TRNSYS validation, Renew. Energy 146 (2020) 1907–1921, https://doi.org/10.1016/J.RENENE.2019.07.075.

[10] A. Lashin, Analysis of thermal performance a heat pipe for concentrated photovoltaic cooling, J Radiat Res Appl Sci 16 (2023) 100606, https://doi.org/10.1016/J.JRRAS.2023.100606.

[11] D. Singh, H. Chaubey, Y. Parvez, A. Monga, S. Srivastava, Performance improvement of solar PV module through hybrid cooling system with thermoelectric coolers and phase change material, Sol. Energy 241 (2022) 538–552, https://doi.org/10.1016/J.SOLENER.2022.06.028.

[12] H.M.S. Bahaidarah, A.A.B. Baloch, P. Gandhidasan, Uniform cooling of photovoltaic panels: a review, Renew. Sustain. Energy Rev. 57 (2016) 1520–1544, https://doi.org/10.1016/J.RSER.2015.12.064.

[13] Austin J. Kluth. 6.8.1 Kluth A. Using Water as a Coolant to Increase Solar Panel n.d.

[14] A. Hadipour, M. Rajabi Zargarabadi, S. Rashidi, An efficient pulsed- spray water cooling system for photovoltaic panels: experimental study and cost analysis, Renew. Energy 164 (2021) 867–875, https://doi.org/10.1016/J.RENENE.2020.09.021.

[15] M.H. Shahverdian, A. Sohani, H. Sayyaadi, S. Samiezadeh, M.H. Doranehgard, N. Karimi, et al., A dynamic multi-objective optimization procedure for water cooling of a photovoltaic module, Sustain. Energy Technol. Assessments 45 (2021), https://doi.org/10.1016/j.seta.2021.101111.

[16] COMSOL Multiphysics, Heat transfer: conservation of energy. https://www.comsol.com/multiphysics/heat-transfer-conservation-of-energy, 2018. (Accessed 20 May 2024).

[17] J. Zhou, X. Ma, X. Zhao, Y. Yuan, M. Yu, J. Li, Numerical simulation and experimental validation of a micro-channel PV/T modules based direct-expansion solar heat pump system, Renew. Energy 145 (2020) 1992–2004, https://doi.org/10.1016/J.RENENE.2019.07.049.

[18] A.S. Joshi, A. Tiwari, G.N. Tiwari, I. Dincer, B.V. Reddy, Performance evaluation of a hybrid photovoltaic thermal (PV/T) (glass-to-glass) system, Int. J. Therm. Sci. 48 (2009) 154–164, https://doi.org/10.1016/J.IJTHERMALSCI.2008.05.001.

[19] J.A. Duffie, W.A. Beckman, Solar Engineering of Thermal Processes, Wiley, 2013.

[20] S. Yoon, J. Seo, M. Choi, B.J. Lee, Enhanced photovoltaic efficiency through radiative cooling augmented by a thermosyphon effect, Energy Convers. Manag. 268 (2022), https://doi.org/10.1016/j.enconman.2022.116046.

[21] M. Alktranee, M.A. Shehab, Z. Németh, P. Bencs, K. Hernadi, T. Koós, Energy and exergy assessment of photovoltaic-thermal system using tungsten trioxide nanofluid: an experimental study, International Journal of Thermofluids 16 (2022) 100228, https://doi.org/10.1016/J.IJFT.2022.100228.

[22] A.M.A. Alshibil, I. Farkas, P. Víg, Multi-aspect approach of electrical and thermal performance evaluation for hybrid photovoltaic/thermal solar collector using TRNSYS tool, International Journal of Thermofluids 16 (2022) 100222, https://doi.org/10.1016/J.IJFT.2022.100222.

[23] R. Nasrin, M. Hasanuzzaman, N.A. Rahim, Effect of high irradiation on photovoltaic power and energy, Int. J. Energy Res. 42 (2018) 1115–1131, https://doi.org/10.1002/er.3907.

[24] A. Parthiban, K.S. Reddy, B. Pesala, T.K. Mallick, Effects of operational and environmental parameters on the performance of a solar photovoltaic-thermal collector, Energy Convers. Manag. 205 (2020), https://doi.org/10.1016/j.enconman.2019.112428.

[25] O. Rejeb, H. Dhaou, A. Jemni, A numerical investigation of a photovoltaic thermal (PV/T) collector, Renew. Energy 77 (2015) 43–50, https://doi.org/10.1016/J.RENENE.2014.12.012.

[26] T. Ma, M. Li, A. Kazemian, Photovoltaic thermal module and solar thermal collector connected in series to produce electricity and high-grade heat simultaneously, Appl. Energy 261 (2020) 114380, https://doi.org/10.1016/J.APENERGY.2019.114380.

[27] I. Kaaya, J. Ascencio-Vásquez, K.A. Weiss, M. Topič, Assessment of uncertainties and variations in PV modules degradation rates and lifetime predictions using physical models, Sol. Energy 218 (2021) 354–367, https://doi.org/10.1016/j.solener.2021.01.071.

[28] I. Kaaya, M. Koehl, A.P. Mehilli, S. De Cardona Mariano, K.A. Weiss, Modeling outdoor service lifetime prediction of PV modules: effects of combined climatic stressors on PV module power degradation, IEEE J. Photovoltaics 9 (2019) 1105–1112, https://doi.org/10.1109/JPHOTOV.2019.2916197.

[29] EnergyPlus Weather Data Available online: energyplus.net/weather n.d.

[30] A. Jha, P.P. Tripathy, Heat transfer modeling and performance evaluation of photovoltaic system in different seasonal and climatic conditions, Renew. Energy 135 (2019) 856–865, https://doi.org/10.1016/j.renene.2018.12.032.

[31] C. Guo, J. Ji, W. Sun, J. Ma, W. He, Y. Wang, Numerical simulation and experimental validation of tri-functional photovoltaic/thermal solar collector, Energy 87 (2015) 470–480, https://doi.org/10.1016/j.energy.2015.05.017.

[32] A. Bala Subramaniyan, R. Pan, J. Kuitche, G. TamizhMani, Quantification of environmental effects on PV module degradation: a physics-based data-driven modeling method, IEEE J. Photovoltaics 8 (2018) 1289–1296, https://doi.org/10.1109/JPHOTOV.2018.2850527.

[33] F. Faraz Ahmad, Z. Said, A. Amine Hachicha, Experimental performance evaluation of closed loop mist/fog cooling system for photovoltaic module application, Energy Convers. Manag. X 14 (2022), https://doi.org/10.1016/j.ecmx.2022.100226.

[34] M. Dida, S. Boughali, D. Bechki, H. Bouguettaia, Experimental investigation of a passive cooling system for photovoltaic modules efficiency improvement in hot and arid regions, Energy Convers. Manag. 243 (2021), https://doi.org/10.1016/j.enconman.2021.114328.

[35] S. Nižetić, D. Čoko, A. Yadav, F. Grubišić-Čabo, Water spray cooling technique applied on a photovoltaic panel: the performance response, Energy Convers. Manag. 108 (2016) 287–296, https://doi.org/10.1016/J.ENCONMAN.2015.10.079.